# Supporting Information for

## Inhibition of the P3-O3 phase transition via local symmetry tuning in P3-type layered cathodes for ultra-stable sodium storage

Ya-Nan Zhou[a], Zichun Xiao[a], Duzhao Han[a], Suning Wang[a,b], Jinniu Chen[a], Wei Tang [a, *], Mingyu Yang[a], Le Shao[c], Chengyong Shu[a], Weibo Hua [a,b,*], Dezhong Zhou[a, *], Yuping Wu[d]

[a] School of Chemical Engineering and Technology, Xi'an Jiaotong University, Xi'an, Shaanxi, 710049, China
[b] Institute for Applied Materials (IAM), Karlsruhe Institute of Technology (KIT), Hermann-von-Helmholtz-Platz 1, D-76344 Eggenstein-Leopoldshafen, Germany
[c] Shaanxi Coal Chemical Industry Technology Research Institute Co., Ltd., Xi'an, Shaanxi, 710049, China
[d] School of Energy and Environment, Southeast University, Nanjing 210096, China

* E-mail: tangw2018@xjtu.edu.cn; weibo.hua@xjtu.edu.cn; dezhong.zhou@mail.xjtu.edu.cn

**Experimental Section**

*Materials synthesis.* The cathodes of P3-$Na_{2/3}Ni_{1/3}Mn_{2/3}O_2$ and P3-$Na_{2/3}Li_{1/9}Ni_{5/18}Mn_{1/2}Ti_{1/6}O_2$ were prepared through sol-gel methods. Stoichiometric amount of $NaNO_3$ (AR, 98%), $Ni(NO_3)_2$ (AR, 98%), $Mn(NO_3)_2$·50% (AR, 98%), $LiNO_3$ (AR, 98%) and $C_{16}H_{36}O_4Ti$ (AR, 98%) were dissolved in the water, subsequently adding the aqueous solution of citric acid and then stirring under 70 ℃ to evaporate water until forming a viscous gel. After drying the gel at 120℃ for 24 h, the resulted precursor was calcined in air at 450 ℃ for 6 h and 700 ℃ for 12 h to obtain target materials. The resulting samples were transferred into glove box filled with Ar ($H_2O$, $O_2$ < 1 ppm) until use. The hard carbon was purchased from Kuraray.

*Materials characterization.* The crystal structures of the cathodes were determined by X-ray diffractometer (XRD) (Bruker D8 Advance) with Cu Kα radiation. The Rietveld refinement of X-ray data was performed using TOPAS software based on the Rietveld method. The *in situ* XRD patterns during the first charge and discharge process were collected at the beamline P02.1, storage ring PETRA-III, at DESY (Deutsches Elektronensynchrotron) in Hamburg, Germany. The morphologies of the materials were examined with MAIA3 LMH scanning electron microscopy (SEM). The microstructure and element information of the layered cathode were investigated by high-resolution transition electron microscopy (HRTEM) and energy-dispersive spectroscopy (EDS) via using TEM (JEOL JEM-F200). The X-ray photoelectron spectra (XPS) of the materials were recorded on Thermo Fisher ESCALAB Xi+. The *in situ* XAS measurements were performed at the P64 beamline, storage ring PETRA-III at Deutsches Elektronensynchrotron (DESY) in Hamburg, Germany.

*Electrochemical measurements.* The working cathode electrodes and hard carbon electrodes were prepared by mixing the active materials, Super P and polyvinylidene fluoride (PVDF) with a weight ratio of 7:2:1 and 8:1:1. Then, casting the slurry on aluminum foil and dried at 70 °C under vacuum overnight. 1M $NaClO_4$ in polycarbonate (PC) with the addition of

5% fluoroethylene carbonate (FEC) was used as the electrolyte. The loading of active materials is about ~2 mg $cm^{-2}$. The CR2032 coin-type batteries were assembled by sandwiching the Whatman glass fiber separator between the electrode and sodium metal in a glove box filled with Ar ($H_2O$, $O_2$ < 1 ppm). As for the sodium full batteries, the hard carbon used as the anode and the weight ratio of cathode and anode was balanced by considering the corresponding reversible capacities. In detail, N/P ratio of assembled sodium full batteries with P3-NaLNMT cathode and hard carbon anode is 1:1.1. Before assembling the sodium full batteries, the hard carbon was pre-cycled. The electrochemical performance of the half batteries and full batteries was investigated on Neware BTS-610 instrument at room temperature within a voltage window of 2.5–4.15 V vs. $Na/Na^+$. During the galvanostatic intermittent titration technique (GITT) tests, the battery was charged at 0.1C for 30 minutes, followed by open-circuit relaxation of 10 h. Cyclic voltammetry (CV) measurements were carried out using Princeton electrochemical workstation.

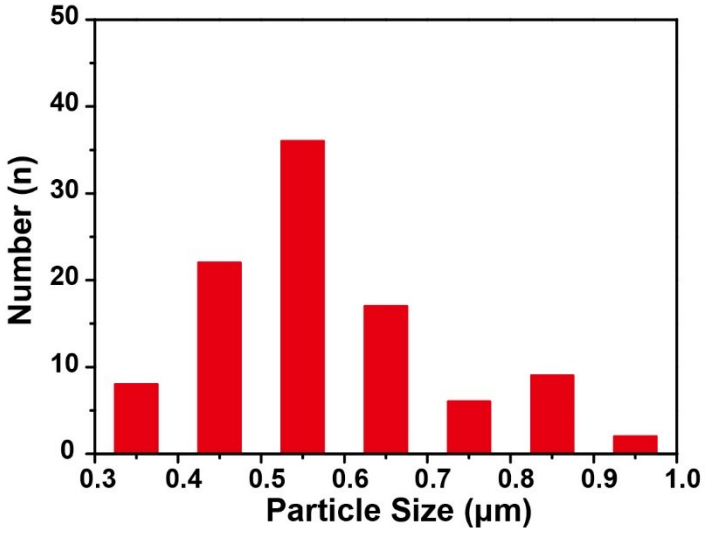


**Fig. S1** The particle size distribution of P3-NaLNMT cathodes.

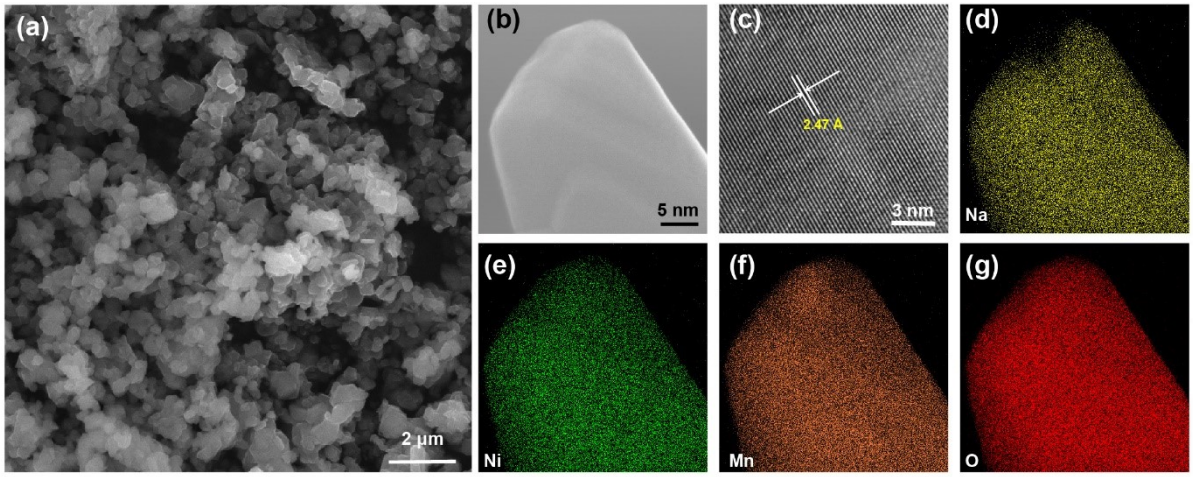


**Fig. S2** SEM images (a), HRTEM images (b, c) and EDS mapping images (d-g) of P3-NaNM cathodes.

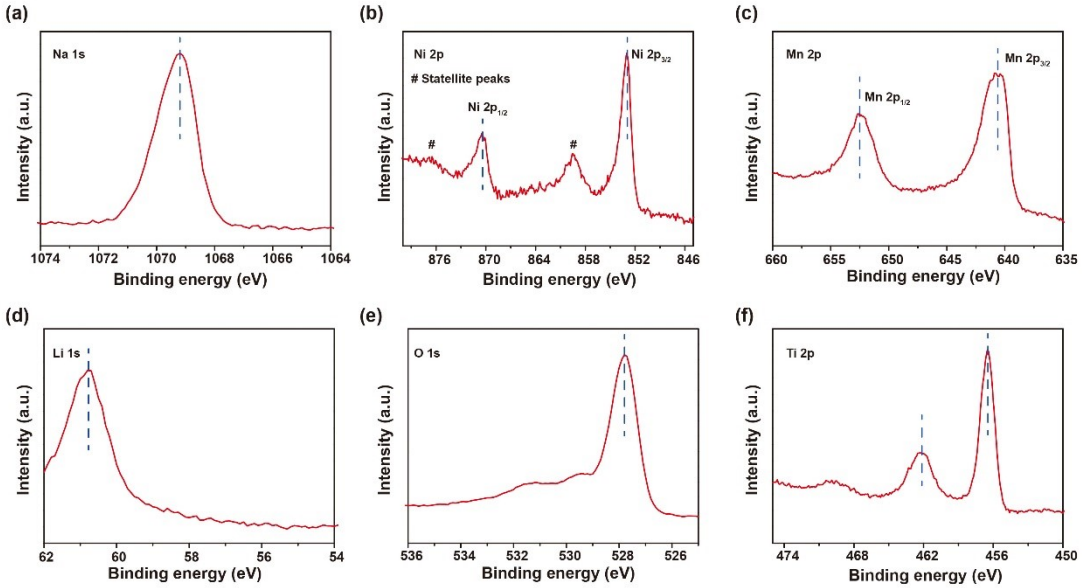


**Fig. S3** The XPS spectra of P3-NaLNMT samples: (a) Na 1s, (b) Ni 2p, (c) Mn 2p, (d) Li 1s, (e) O 1s and (f) Ti 2p.

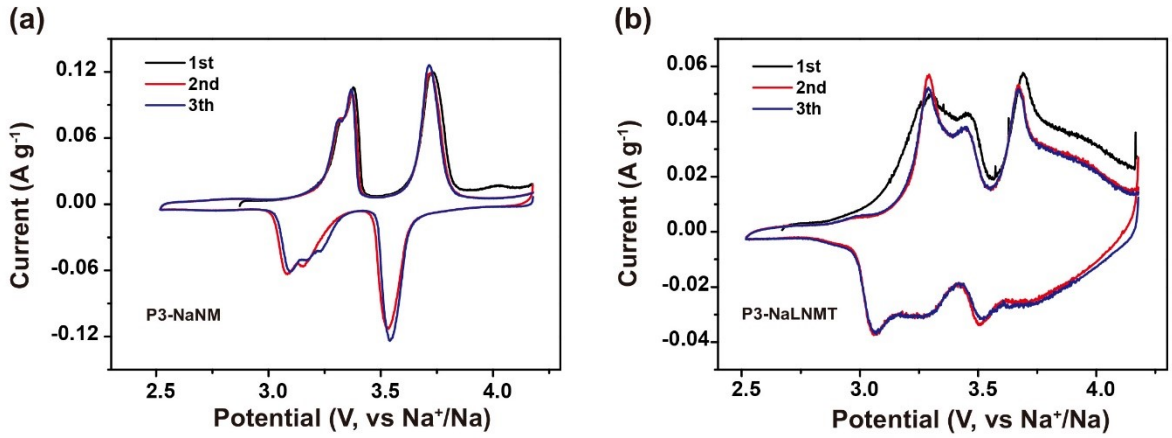


**Fig. S4** CV curves of P3-NaNM (a) and P3-NaLNMT (b) cathodes.

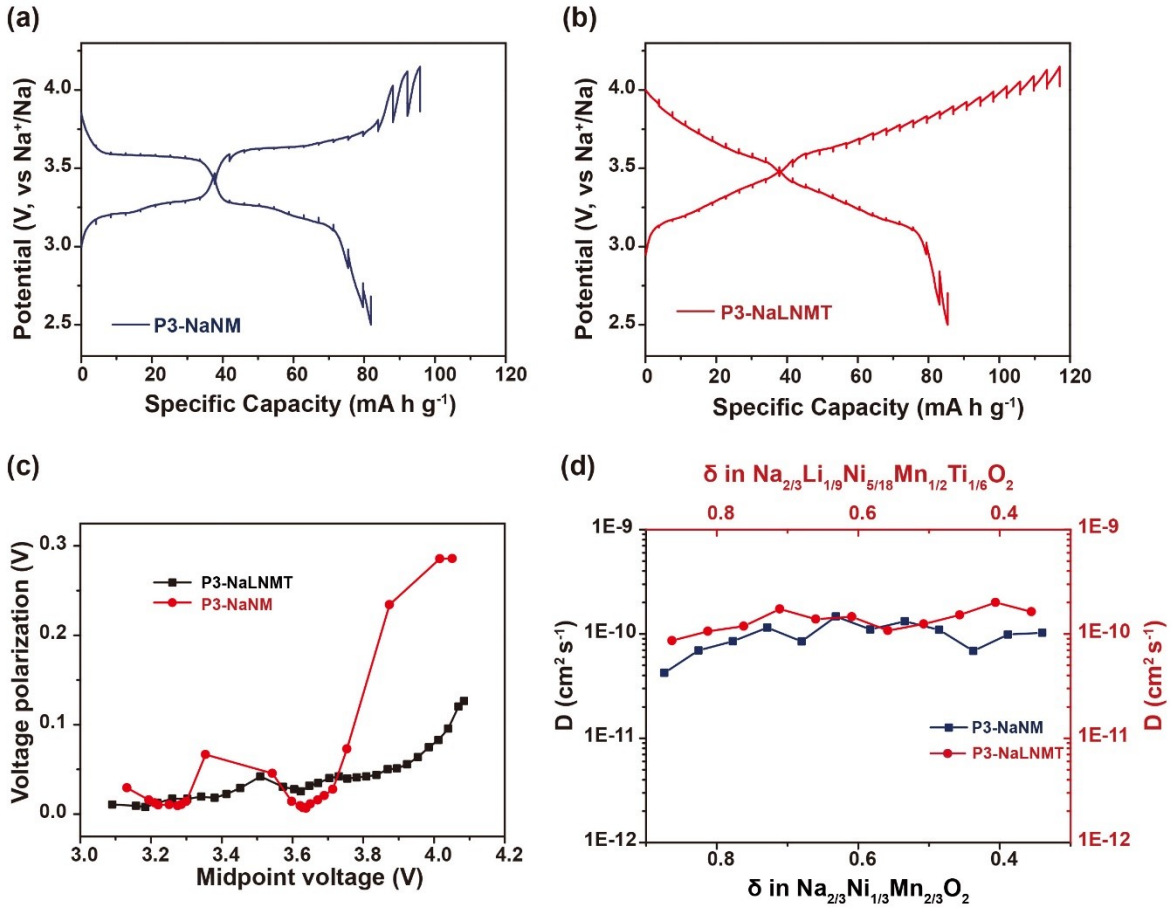


**Fig. S5** GITT profiles of the (a) P3-NaNM and (b) P3-NaLNMT cathodes during the voltage window of 2.5–4.15V. (c) Corresponding voltage polarization of the two cathodes. (d) The calculated diffusion coefficients from GITT.

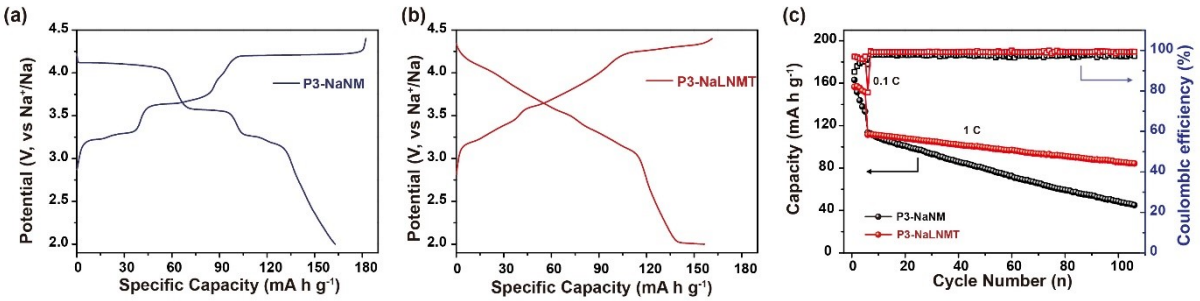


**Fig. S6** Charge/discharge profiles of P3-NaNM (a) and (b) P3-NaLNMT at 0.1C, and cycling performance at 1C (c) in the voltage window of 2–4.4 V.

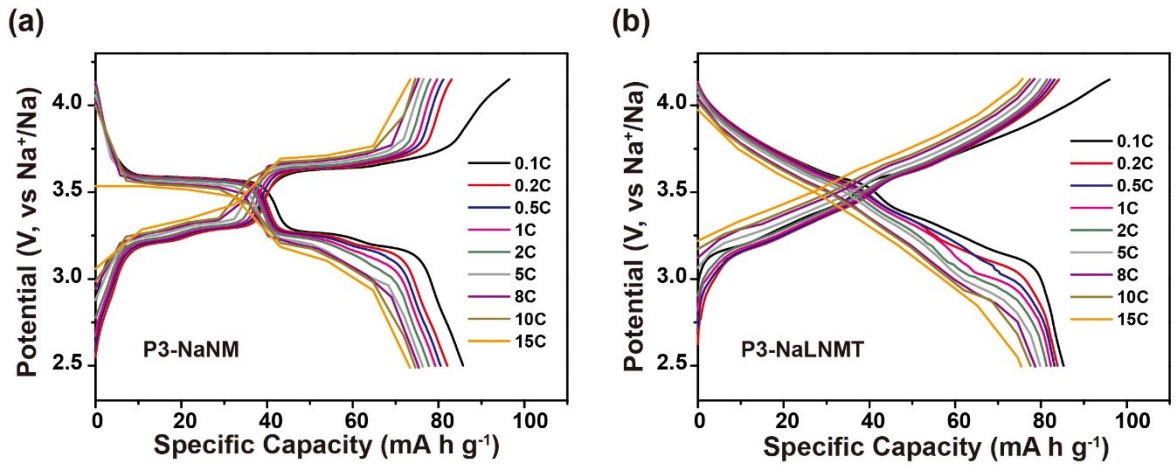


**Fig. S7** Charge/discharge profiles of P3-NaNM (a) and (b) P3-NaLNMT at different current densities.

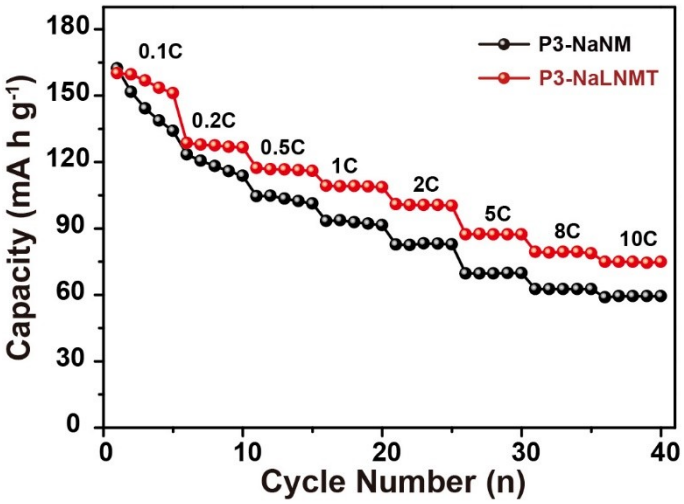


**Fig. S8** Rate performance of P3-NaNM and P3-NaLNMT at the voltage of 2–4.4 V.

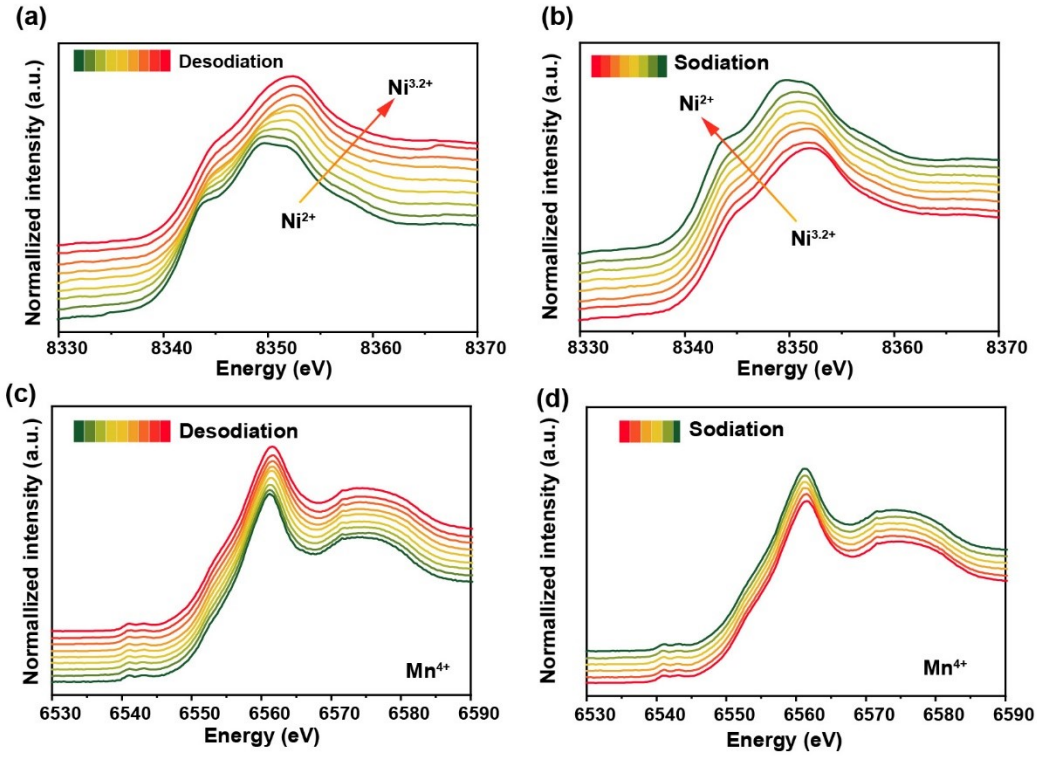


**Fig. S9** Charge /Discharge compensation mechanism: *In situ* XANES spectra at Ni K-edge (a), (b) and Mn K-edge (c), (d) of P3-NaLNMT cathodes.

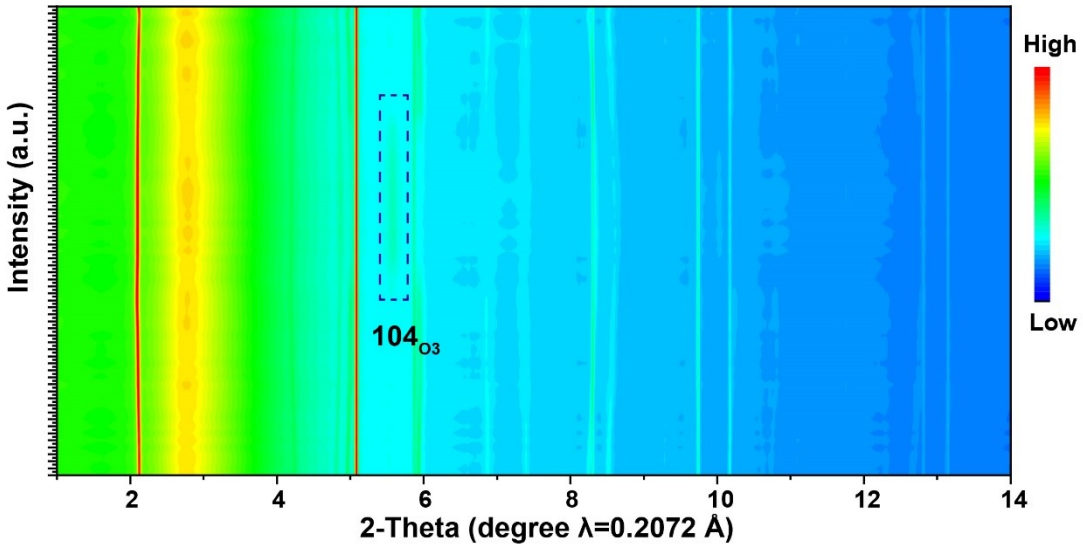


**Fig. S10** Corresponding intensity contour maps of P3-NaNMcathode concerning the evolution of the diffraction peaks of 1–14° (λ= 0.2072 Å).

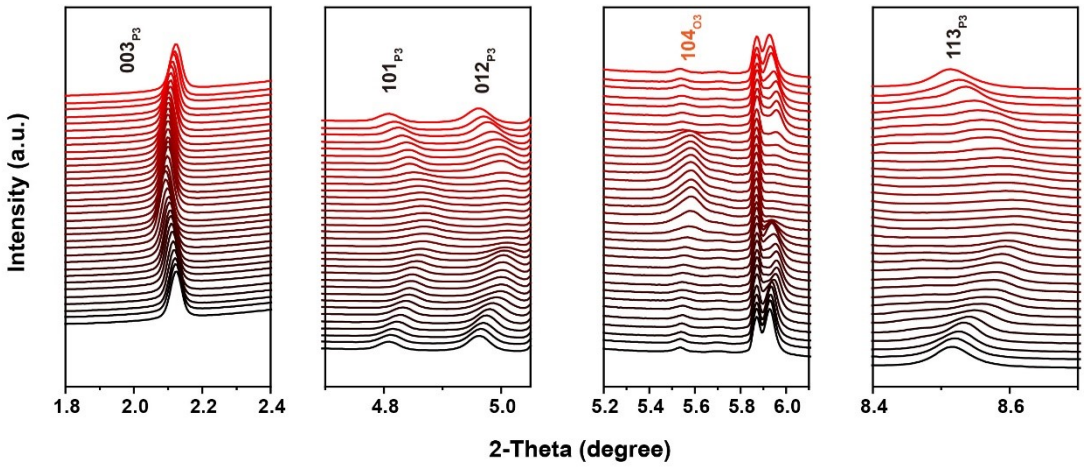


**Fig. S11** Partial *in situ* XRD diffraction peaks of the P3-NaNM cathode.

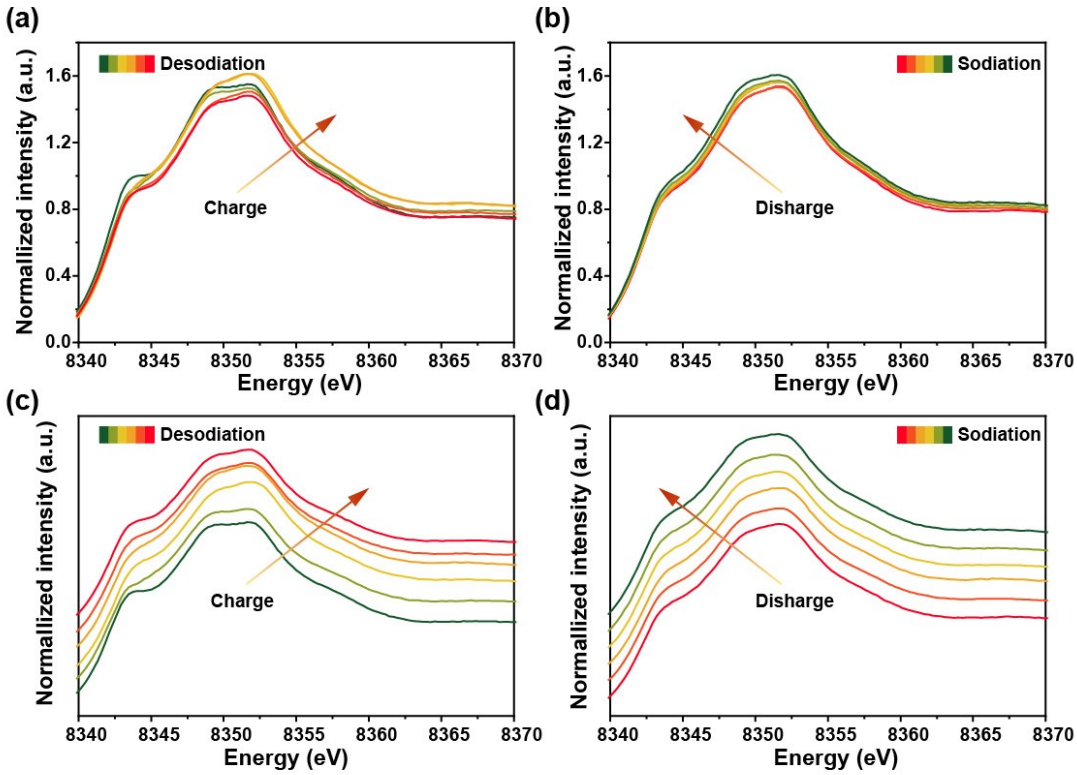


**Fig. S12** Charge (a, c)/Discharge (b, d) compensation mechanism: *In situ* XANES spectra at Ni K-edge of P3-NaNM cathodes.

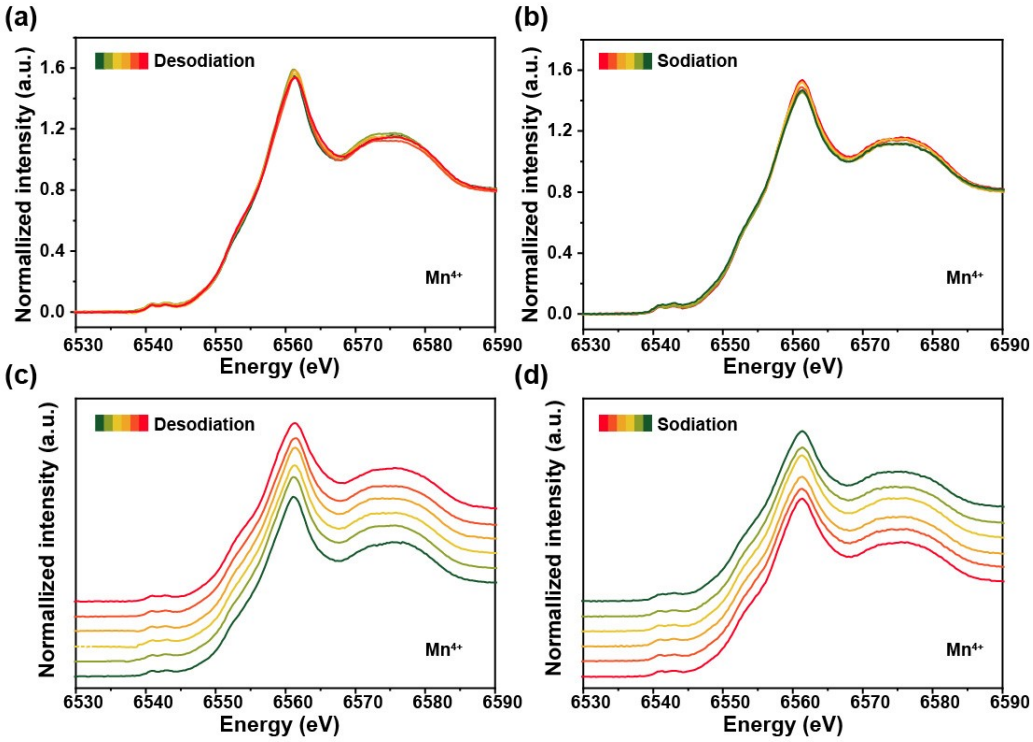


**Fig. S13** Charge (a, c)/Discharge (b, d) compensation mechanism: *In situ* XANES spectra at Mn K-edge of P3-NaNM cathodes.

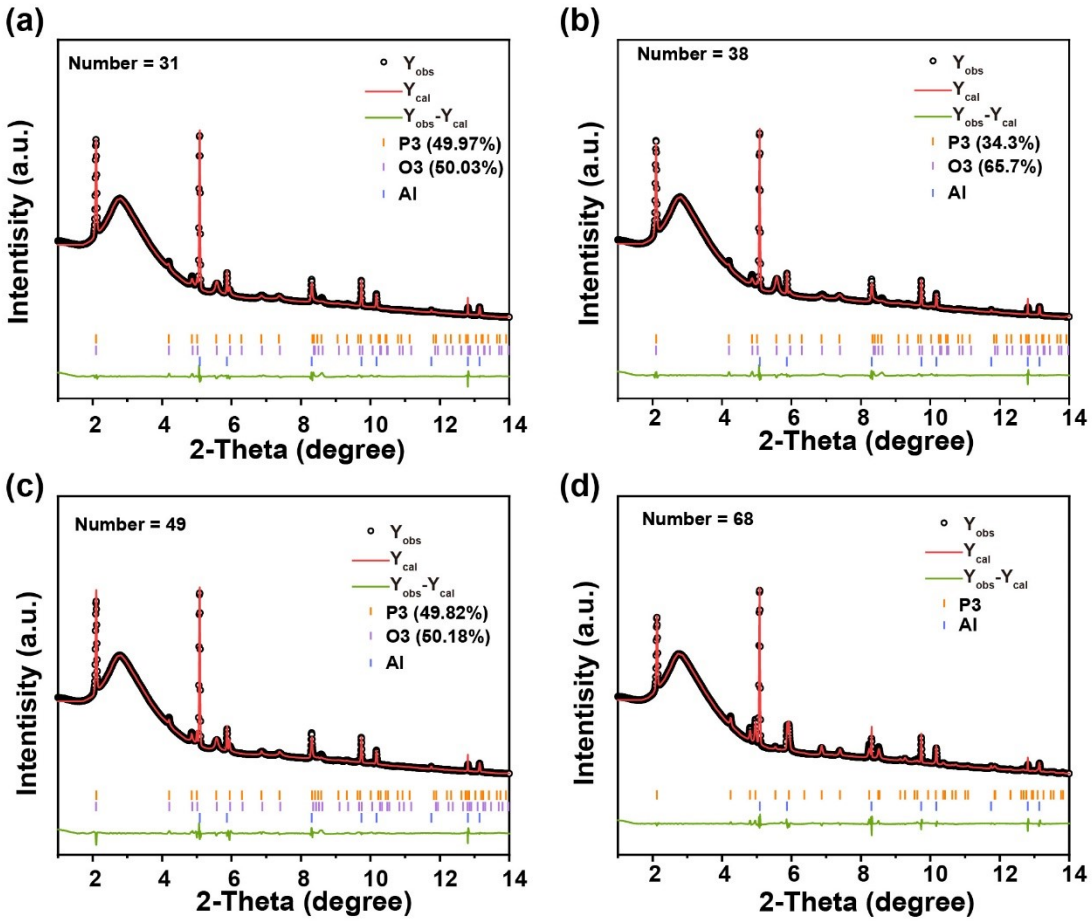


**Fig. S14** Fitted *in situ* X-ray diffractograms (λ= 0.2072 Å) for P3-NaLNMT.

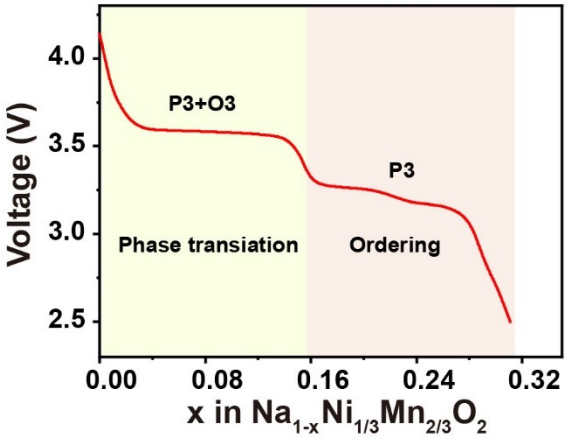


**Fig. S15** Phase transition as a function of sodium content during discharge process.

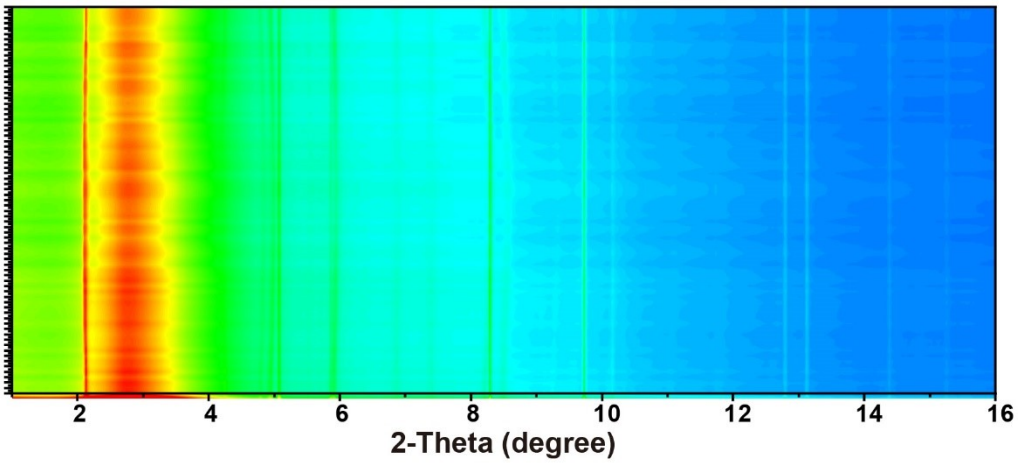


**Fig. S16** Corresponding intensity contour maps of P3-NaLNMT cathode concerning the evolution of the diffraction peaks of 1–16° (λ= 0.2072 Å).

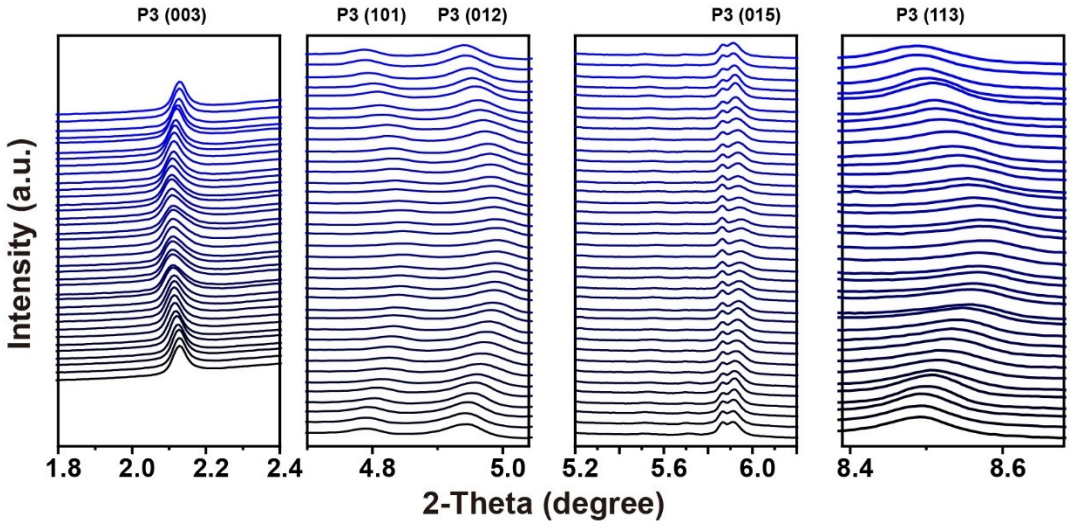


**Fig. S17** Partial *in situ* XRD diffraction (λ= 0.2072 Å) peaks of the P3-NaLNMT cathode.

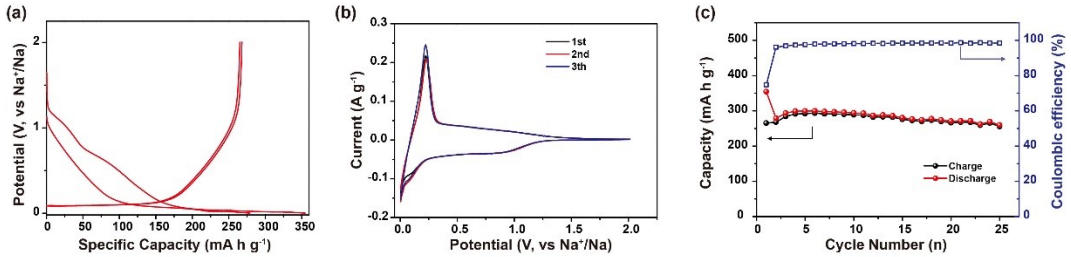


**Fig. S18** Electrochemical performance of hard carbon. Charge-discharge curves at 50 mA $g^{-1}$ over the potential window of 0.001–2.0 V(a), (b) cyclic voltammograms at 0.1 mV $s^{-1}$ and (c) cycling performance at 50 mA $g^{-1}$.

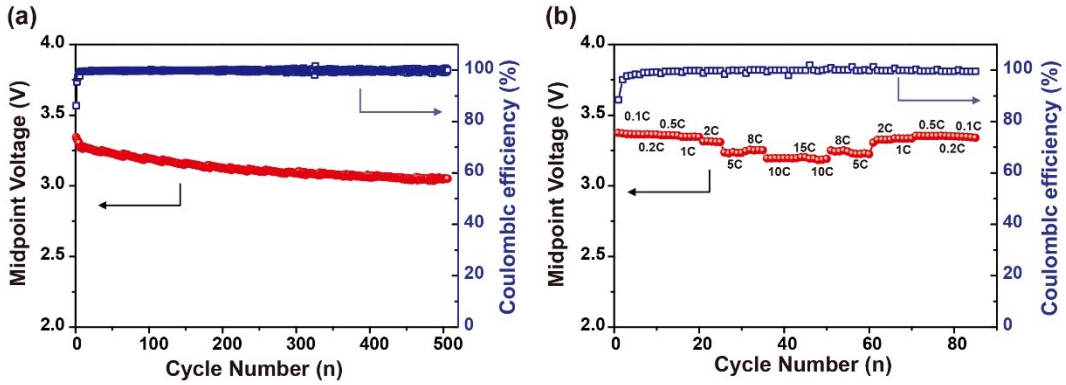


**Fig. S19** Electrochemical performance of Na-ion full battery. (a) Cycling performance with midpoint voltage. (b) Rate performance at various rates with midpoint voltage in the range of 2.5–4.15 V.

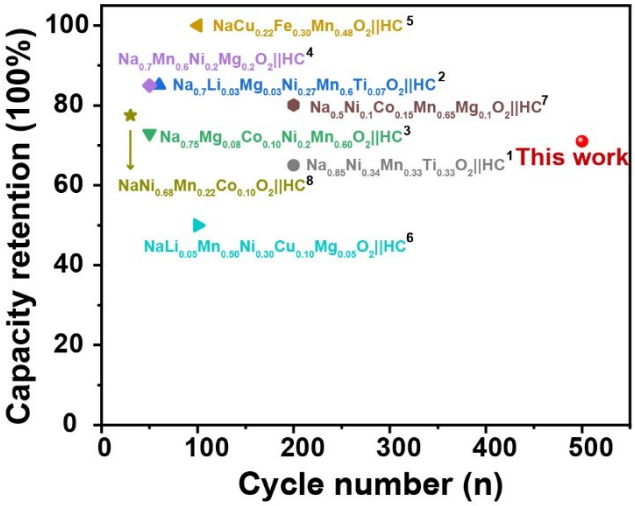


**Fig. S20** Comparison of cycle number and capacity retention between our and other sodium-ion full batteries reported recently. [1-8]

**Table S1.** Structural parameters and atomic position of P3-NaNM from Rietveld refinement.

| **Atom** | **Np** | **x** | **y** | **z** | **Occ.** |
|---|---|---|---|---|---|
| Na | 3 | 0.00000 | 0.00000 | 0.16810 | 0.67 |
| Ni | 3 | 0.00000 | 0.00000 | 0.00000 | 0.33 |
| Mn | 3 | 0.00000 | 0.00000 | 0.00000 | 0.67 |
| O1 | 3 | 0.00000 | 0.00000 | 0.39213 | 1.0 |
| O2 | 3 | 0.00000 | 0.00000 | -0.39210 | 1.0 |
| a = 2.8886(2) Å c = 16.788(9) Å V = 121.32(0) Å$^3$ | | | | | |
| $R_p$ = 5.45 % $R_{wp}$ = 6.82 % GOF: 1.28% | | | | | |

**Table S2.** Structural parameters and atomic position of P3-NaLNMT from Rietveld refinement.

| **Atom** | **Np** | **x** | **y** | **z** | **Occ.** |
|---|---|---|---|---|---|
| Na | 3 | 0.00000 | 0.00000 | 0.16487 | 0.7 |
| Li | 3 | 0.00000 | 0.00000 | 0.00000 | 0.11 |
| Ni | 3 | 0.00000 | 0.00000 | 0.00000 | 0.27 |
| Mn | 3 | 0.00000 | 0.00000 | 0.00000 | 0.5 |
| Ti | 3 | 0.00000 | 0.00000 | 0.00000 | 0.17 |
| O1 | 3 | 0.00000 | 0.00000 | 0.38728 | 1.0 |
| O2 | 3 | 0.00000 | 0.00000 | -0.39214 | 1.0 |
| a = 2.902(1) Å | | c = 16.805(3) Å | | V = 122.57(4) Å$^3$ | |
| $R_p$ = 2.10 % | | $R_{wp}$ = 2.84 % | | GOF: 1.78% | |

**Table S3.** Structural parameters of P3-$Na_x$LNMT obtained from the Ni K-edge EXAFS spectra.

| Scan Number | Ni–O | | |
|---|---|---|---|
| | CN | R(Å) | $\sigma^2$(Å$^2$) |
| 1 | 6 | 2.05045 | 0.00897 |
| 2 | 6 | 2.04465 | 0.00843 |
| 3 | 6 | 2.03034 | 0.00894 |
| 4 | 6 | 2.01553 | 0.01380 |
| 5 | 6 | 1.99340 | 0.01798 |
| 6 | 6 | 1.97040 | 0.02052 |
| 7 | 6 | 1.94289 | 0.01886 |
| 8 | 6 | 1.93056 | 0.01924 |
| 9 | 6 | 1.92386 | 0.02056 |
| 10 | 6 | 1.93327 | 0.01863 |
| 11 | 6 | 1.93847 | 0.01610 |
| 12 | 6 | 1.95078 | 0.01639 |
| 13 | 6 | 1.97392 | 0.01759 |
| 14 | 6 | 1.99047 | 0.01702 |
| 15 | 6 | 2.00630 | 0.01497 |
| 16 | 6 | 2.02924 | 0.00882 |
| 17 | 6 | 2.04663 | 0.00867 |

**Table S4.** Structural parameters of P3-$Na_xLNMT$ obtained from the Mn K-edge EXAFS spectra.

| Scan Number | Mn–O | | |
|---|---|---|---|
| | CN | R(Å) | $\sigma^2$(Å$^2$) |
| 1 | 6 | 1.89183 | 0.00233 |
| 2 | 6 | 1.88776 | 0.00334 |
| 3 | 6 | 1.88532 | 0.00349 |
| 4 | 6 | 1.88312 | 0.00416 |
| 5 | 6 | 1.87693 | 0.00377 |
| 6 | 6 | 1.87115 | 0.00315 |
| 7 | 6 | 1.86284 | 0.00396 |
| 8 | 6 | 1.87043 | 0.00340 |
| 9 | 6 | 1.87490 | 0.00361 |
| 10 | 6 | 1.87831 | 0.00244 |
| 11 | 6 | 1.88059 | 0.00337 |
| 12 | 6 | 1.88262 | 0.00229 |
| 13 | 6 | 1.88371 | 0.00258 |
| 14 | 6 | 1.88538 | 0.00197 |
| 15 | 6 | 1.88776 | 0.00211 |
| 16 | 6 | 1.88978 | 0.00257 |
| 17 | 6 | 1.88998 | 0.00307 |

**Reference.**


1. L. Yu, Z. Cheng, K. Xu, Y.-X. Chang, Y.-H. Feng, D. Si, M. Liu, P.-F. Wang and S. Xu, *Energy Storage Mater*, 2022, **50**, 730-739.
2. Z. Cheng, B. Zhao, Y. J. Guo, L. Yu, B. Yuan, W. Hua, Y. X. Yin, S. Xu, B. Xiao, X. Han, P. F. Wang and Y. G. Guo, *Adv. Energy Mater.*, 2022, **12**,2103461.
3. Y. Shi, Z. Zhang, P. Jiang, A. Gao, K. Li, Q. Zhang, Y. Sun, X. Lu, D. Cao and X. Lu, *Energy Storage Mater*, 2021, **37**, 354-362.
4. Q.-C. Wang, J.-K. Meng, X.-Y. Yue, Q.-Q. Qiu, Y. Song, X.-J. Wu, Z.-W. Fu, Y.-Y. Xia, Z. Shadike, J. Wu, X.-Q. Yang and Y.-N. Zhou, *J. Am. Chem. Soc.*, 2018, **141**, 840-848.
5. L. Mu, S. Xu, Y. Li, Y. S. Hu, H. Li, L. Chen and X. Huang, *Adv Mater*, 2015, **27**, 6928-6933.
6. J. Deng, W.-B. Luo, X. Lu, Q. Yao, Z. Wang, H.-K. Liu, H. Zhou and S.-X. Dou, *Adv. Energy Mater.*, 2018, **8,** 1701610.
7. Y. F. Zhu, Y. Xiao, W. B. Hua, S. Indris, S. X. Dou, Y. G. Guo and S. L. Chou, *Angew Chem Int Ed Engl*, 2020, **59**, 9299-9304.
8. Y. Jin, Y. Xu, B. Xiao, M. H. Engelhard, R. Yi, T. D. Vo, B. E. Matthews, X. Li, C. Wang, P. M. L. Le and J.-G. Zhang, *Adv. Funct. Mater.*, 2022, **32**, 2204995.